Proceedings of the 21st ICSMGE, Vienna, Austria, 14 – 19 June 2026. Pistrol, Adam & Schweiger (eds.)
Published by: ÖGG, Austrian Society for Geomechanics, Salzburg, Austria, ISBN 978-3-9503898-4-5
https://doi.org/10.53243/ICSMGE2026-922

Large deformation coupled hydro-mechanical CEL analysis of cone penetration into dense sand

Ahmad Foroutan Kalourazi, Tingfa Liu, Andrea Diambra, George Mylonakis
School of Civil, Aerospace and Design Engineering, University of Bristol, Bristol, UK,
ahmad.foroutankalourazi@bristol.ac.uk

Yinghui Tian
Department of Infrastructure Engineering, The University of Melbourne, Melbourne, Victoria, Australia

ABSTRACT: Geotechnical large-deformation problems pose significant challenges for classical finite element methods due to mesh distortion, contact complexities and other numerical issues. The Coupled Eulerian-Lagrangian (CEL) method has been widely recognised as a robust approach for tackling these challenges. However, the method is primarily limited to total stress analysis, which constrains its applications for addressing effective stress and consolidation problems in saturated soils. This study employs a coupled hydro-mechanical CEL framework based on a pore pressure-thermal analogy and investigates its applicability for modelling cone penetration into dense sands with an advanced hypoplastic constitutive model. The modelling results indicate significant increases in cone resistance and (negative) excess pore pressure with the increases in penetration velocity, reflecting combined consolidation and viscous effects that can be interpreted within a drainage backbone curve framework. Radial effective stresses build up at any given depth as cone tip approaches and then reduce sharply as the tip advances. Their post-penetration distributions depend critically on the spatial position relative to the cone tip and on the local rate-dependent cone resistances. The coupled CEL method provides a robust framework for simulating large-deformation penetration and installation problems in challenging geomaterials.

KEYWORDS: Large deformation, Coupled Eulerian-Lagrangian (CEL) method, Hydro-Mechanical Coupled analysis, pile foundation.

1 INTRODUCTION

Installation of pile foundations typically involves large deformations and complex hydro-mechanical coupling phenomena that affect driving resistance and pile's short- and long-term axial capacities. Soil states and stresses acting around piles post-installation could differ markedly from those applied at in-situ and their accurate prediction remains challenging in pile analysis and design. Extensive field investigations and model studies with instrumented piles have found correlations between local shaft and base resistances with cone tip resistance, normalised pile tip depth and other factors, leading to improved CPT-based axial capacity methods for driven piles in sands, clays and chalk (Jardine et al., 2005; Jardine 2023; Liu et al., 2025).

Numerical modelling offers a complementary means to field and model experiments of evaluating installation effects and assessing pile capacities (Yi et al., 2012). However, conventional Lagrangian finite element (FEM) method often encounters severe mesh distortion when applied in large deformation problems (Qiu et al., 2011). Advanced numerical methods have been developed to tackle these limitations, including discontinuum (such as discrete element modelling) and continuum approaches. The latter can be further divided based on material discretisation into particle-based methods, such as MPM and PFEM, and mesh-based methods, including RITSS, EALE and CEL (Augarde et al., 2021). These methods have been widely applied in modelling penetration problems.

The Coupled Eulerian–Lagrangian (CEL) approach has proven to be an effective tool for simulating large-deformation problems. Its implementation in commercial software such as Abaqus/Explicit and LS-DYNA, combined with the use of explicit time integration, has made CEL particularly suitable for pile driving and other dynamic penetration problems. However, conventional CEL is restricted to total stress analyses. To overcome this limitation, Hamann et al. (2015) developed a coupled hydro-mechanical CEL framework based on a pore pressure–thermal analogy. This framework was later extended by Staubach et al. (2020, 2021) to cover the modelling scenarios of high wave frequency and hydraulic conductivity. Kalourazi et al. (2025) demonstrated how the coupled CEL approach incorporating an advanced hypoplastic model can be applied for the prediction of cone resistances under variable penetration rates. Building on this earlier research, the current study considers modelling of variable rate cone penetration process in dense sands with particular focuses on the evolution and distribution of excess pore water pressure and radial effective stress as the sands undergo large strain, dilatant shearing. The modelling outcomes have important application and implication for evaluating installation effects of piles in sands and improving the CPT and effective stress based axial capacity methods for pile foundations in unconventional geomaterials.

2 CONVENTIONAL AND HYDRO-MECHANICAL COUPLED CEL

The Coupled Eulerian–Lagrangian (CEL) method combines Eulerian and Lagrangian domains within a single model (Noh, 1963; Benson, 1992). As illustrated in Figure 1, the Eulerian elements are assigned to regions undergoing large deformations, allowing material to pass through a fixed mesh and thereby avoiding mesh distortion. The Lagrangian elements represent areas with minor deformations where the mesh moves with the material. The solution is advanced through a time-stepping scheme consisting of a Lagrangian step to compute displacements, followed by a remapping step to restore the Eulerian mesh. Interaction between the domains is managed by using a penalty-based general contact algorithm which enables the Lagrangian mesh to move freely within the Eulerian mesh and provides robust handling of complex soil–structure interactions. The CEL method employs explicit time integration that avoids iterative solvers but requires small time steps dictated by material stiffness and the smallest element size, making it particularly suitable for modelling dynamic and large-deformation problems (Dassault Systèmes, 2023). However, the method's implementation within Abaqus/Explicit and other software packages is largely restricted to total stress

analyses and cannot model directly problems involving effective stress or pore water pressure (Wang et al., 2015).

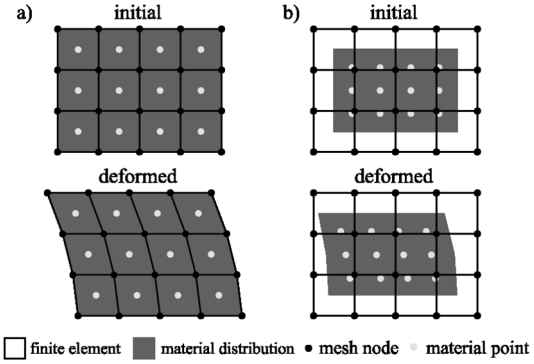

Figure 1. Initial and deformed domain configurations: (a) Lagrangian (b) Eulerian (after Konkol, 2014).

The coupled hydro-mechanical CEL framework adopted in this study was proposed by Hamann et al. (2015) based on the analogy between fluid flow and heat transfer, noting both seepage and thermal fields are governed by convection–diffusion equations of similar forms (Zienkiewicz and Shiomi, 1984). In this approach, the water mass balance equation, which includes Darcy's law (Equation 1), is replaced by the thermal energy balance equation, which incorporates Fourier's law (Equation 2):

$$\frac{n}{K_w}\Delta\dot{p}_w + \frac{k_i}{\mu^l}[-\nabla\Delta p_w] - \frac{k_i}{\mu^l}div(\ddot{u}_s) + div(\dot{u}_s) = 0 \quad (1)$$

$$\rho c\dot{\theta} + \lambda\, div[-\nabla\theta] + \dot{m}_\theta = 0 \quad (2)$$

where n is the volume fraction of pore fluid, K_w (Pa) is the bulk modulus of the fluid, $\dot{u}_s$ (m/s) is the velocity of the solid, $\ddot{u}_s$ (m^2/s) is the acceleration of the solid, Δp_w (Pa) represents excess pore pressure, k_i (m^2) is intrinsic permeability, μ^l (Pa.s) signifies dynamic viscosity phase, ρ (kg/m^3) is density, λ (W/(m·K)) is thermal conductivity, c (J/(kg·K)) denotes specific heat and m_θ represents internal heat energy production (J/(m^3·K)). Three analogous terms can be identified: (i) the first term of Eq.1 that represents water mass changes due to fluid compressibility corresponds to the changes in internal heat energy per unit volume in Eq.2; (ii) the second term of Eq.1 in relation to pore water diffusion is analogous to heat conduction in Eq.2; (iii) the third term of Eq. 1 that represents water mass change required to compensate for the straining of the solid skeleton corresponds to internal heat energy generation in Eq 2.

By substituting these corresponding terms, this framework establishes a set of analogous parameters. Thermal conductivity is equivalent to intrinsic permeability divided by dynamic viscosity, and specific heat corresponds to the volume fraction of pore fluid divided by the product of bulk modulus of water and mixture density:

$$\lambda = \frac{k_i}{\mu^l}, c = \frac{n}{K_w\rho} \quad (3)$$

Finally, temperature is used as a proxy for excess pore pressure, allowing for the simulation of coupled hydro-mechanical problems within the CEL framework:

$$\theta = \Delta p_w \quad (4)$$

By utilising a dynamic temperature–displacement approach, Abaqus/Explicit sequentially solves the momentum balance and heat conduction equations. A user-defined VUMAT subroutine was introduced that incorporates the stress–strain relationships and the coupling between the solid and pore water phases into the simulation.

3 NUMERICAL AND CONSTITUTIVE MODEL

Three-dimensional cone penetration models were established to reproduce the soil and test conditions applied in the centrifuge tests by Stapelfeldt et al. (2020) performed with the UWA fine silica sand (Chow et al., 2019).

As shown in Figure 2, one-quarter of the model was simulated considering the axis-symmetry of the problem. The cone penetrometer was modelled as a rigid body using C3D8R Lagrangian elements with a 0.63 m diameter, 60° tip angle and 8.0 m final penetration depth. The soil domain was modelled using EC3D8RT Eulerian elements, with a diameter of 50 m and a height of 85 m. The top 1 m (blue) represents void, while the remaining 84 m (brown) denotes soil, as distinguished in Figure 2. These dimensions were selected to minimise boundary effects during fast penetration. Coarser meshes were applied in the outer regions using the sweep and advancing front methods to reduce computational cost, while finer, structured meshes were applied near the cone shaft and beneath its tip to ensure the accuracy in capturing soil-cone interaction mechanisms. The adopted model geometry and meshing scheme effectively dampened wave reflections without significantly increasing simulation time. Normal contact was modelled using a general contact method with hard pressure–overclosure and a penalty approach for normal behaviour (Dassault Systèmes, 2023). Tangential contact followed a Coulomb friction model with a coefficient of 0.18 and a shear stress limit of 12 kPa. Simulations were run on the University of Bristol's high-performance computing (HPC) system using 28 cores operating at a base frequency of 2.4 GHz.

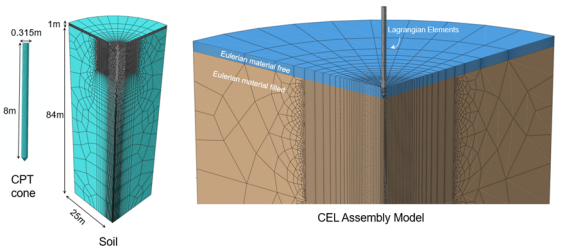

Figure 2. Geometry and mesh of the CEL model for cone penetration

An advanced hypoplastic constitutive model with intergranular strain (Niemunis and Herle, 1997) was incorporated in the hydro-mechanical CEL framework to capture the complex, non-linear behaviour of sand during large-deformation cone penetration. Granular soils exhibit strongly non-linear and inelastic behaviour that cannot be represented by simple linear elastic models. During cone penetration, the soil beneath cone tip is highly compressed, while the material around the shaft is displaced laterally, creating localised zones of compaction and loosening. These mechanisms significantly influence the generation and dissipation of excess pore pressures in fully or partially drained conditions. The hypoplastic model, originally proposed by von Wolffersdorff (1996) and later extended by Niemunis and Herle (1997), captures stress- and density-dependent stiffness, dilatancy and contraction, volumetric behaviour, and different stiffnesses for loading and unloading. The intergranular strain extension further enables the modelling of small-strain stiffness, hysteretic response and other complex cyclic loading conditions. The constitutive model can be expressed in a rate-type formulation defined by the tensorial function:

$$\dot{T} = M(T, e, \delta) : D \quad (5)$$

where $\dot{T}$ is the objective Jaumann stress rate, M is a fourth-order constitutive tensor, T is current Cauchy stress, e is void ratio, δ is intergranular strain, and D is strain-rate tensor.

The input model parameters listed in Table 1 were adopted from Bienen et al. (2011) based on the calibration against extensive laboratory element test results.

Table 1. Hypoplastic model parameters for fine silica sand (adopted from Bienen et al., 2011)

Parameter	Value	Description
φ_c	30	Critical friction angle [°]
h_s	1354	Granular hardness [MPa]
n	0.34	Barotropy exponent
e_{d0}	0.49	Minimum void ratio at zero pressure
e_{c0}	0.79	Critical void ratio at zero pressure
e_{i0}	0.87	Maximum void ratio at zero pressure
α	0.18	Dilatancy exponent
β	1.27	Pyknotropy exponent
m_R	5.16	Stiffness factor (180°)
m_T	3.07	Stiffness factor (90°)
R	1×10^{-4}	Maximum value of intergranular strain
β_R	0.58	Exponent
χ	5.74	Exponent

4 RESULTS AND DISCUSSION

4.1 *Backbone curve and excess pore pressure trends*

Kalourazi et al. (2025) demonstrated how cone resistances increased with penetration rates due to combined consolidation and viscous effects in dense sands. The overall pattern can be interpreted within a drainage framework using a normalised penetration velocity (Chow et al., 2018; Chow et al., 2020).

Cone resistance variations concur with the development of excess pore water pressures. Figure 3 demonstrates the profiles of excess pore pressure measured at the cone shoulder position (u_2) against a non-dimensional velocity $V=vd/c_v$ in a dense fine sand with relative density I_D of 84% and vertical coefficient of consolidation c_v of 3.3×10^{-4} m²/s. The penetration velocities range from 0.01 to 12 m/s, corresponding to normalised velocities from 9.5 to 11,454.5 that cover drained, partially drained and undrained conditions. When penetrating at the lowest velocity, excess pore pressures at the shoulder position remain close to zero, indicating full drainage around the cone tip. As the penetration velocity increases, negative excess pore pressures develop substantially. The highest penetration velocity produces the highest (negative) excess pore pressures, confirming fully undrained conditions with pronounced dilatancy. The results demonstrate a clear rate-dependent pattern that faster penetration limits drainage and amplifies the generation of negative excess pore pressure.

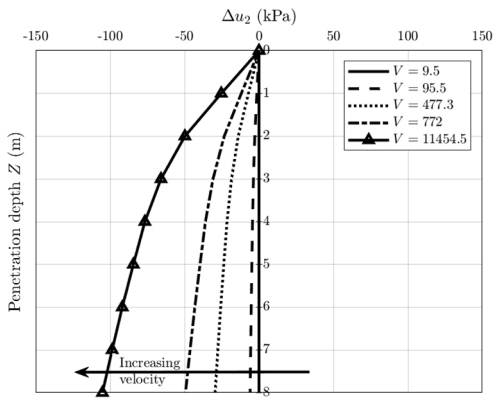

Figure 3. Excess pore pressure variation with depth under different normalised penetration velocities

With reference to the drainage framework, Figure 4 plots the variation of normalised excess pore pressure, $\Delta u_2/\sigma_v'$, against the normalised velocity V. The $\Delta u_2/\sigma_v'$ values were computed and averaged every 0.5 m over the penetration depth of 1 to 8 m. The centrifuge tests and numerical model predictions show generally good match, although discrepancies can be observed in the partially drained regime with $V \approx 10$–250 that may be attributed to uncertainties in the model input parameters and potential variations in the centrifuge test conditions.

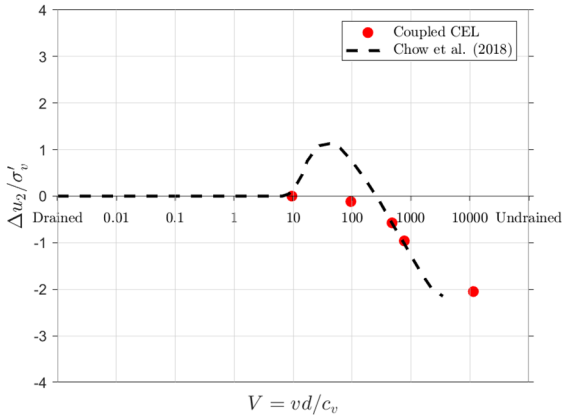

Figure 4. Variation of normalised excess pore pressure ($\Delta u_2/\sigma_v'$) against normalised velocity V

4.2 *Evolution and distribution of radial effective stress*

Establishing the evolution and distribution of soil stresses during and post-pile installation is critical to improving the understanding and modelling of pile behaviour. Figure 5 plots the evolution trends against penetration depth for the radial effective stresses observed at three 'sensor locations' embedded at depths of 1, 4 and 8 m, considering three penetration rates that represent drained, partially drained and undrained conditions. The results indicate a clear pattern of progressive stress build-up in the ground as the pile tip approaches and then sharp reductions that follow as the tip advances. These observations align with the trends observed in calibration chamber tests with instrumented closed-ended piles (Jardine et al., 2013) and large-deformation numerical modelling by ALE and other methods (see Yang et al. (2020) and Ye et al. (2024)). The magnitudes of radial effective stress variations increase with the penetration rates, demonstrating a rate-dependent response in the dense sand undergoing large-strain dilative shearing. The final stabilised radial effective stresses at any given depth deviate from the pre-installation in-situ stresses and vary systematically with the distances to pile tip (h).

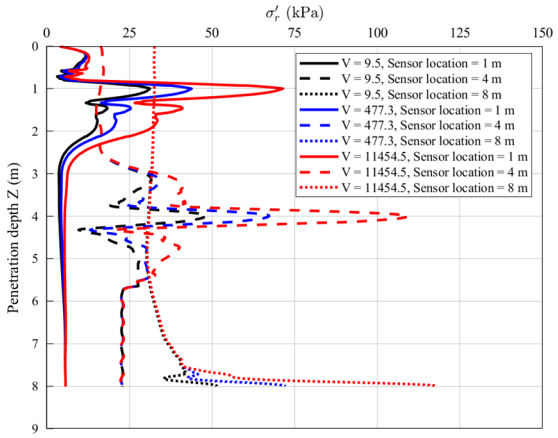

Figure 5. Evolution of effective radial stresses observed at depths of 1, 4 and 8 m below ground level

Figure 6 shows how normalised radial effective stresses (σ_r'/q_c) observed at the shoulder position (h/R = 1.73) vary with normalised radial distances to cone central axis (r/R) immediately after penetrating to a depth of 4 m (Z/R = 12.7). The radial effective stress regime displays maxima at normalised radial distances r/R of ≈ 2. Penetration at greater rates yield higher σ_r' and q_c, resulting in normalised σ_r'/q_c trends that vary seemingly less markedly with the radial distances to cone shaft.

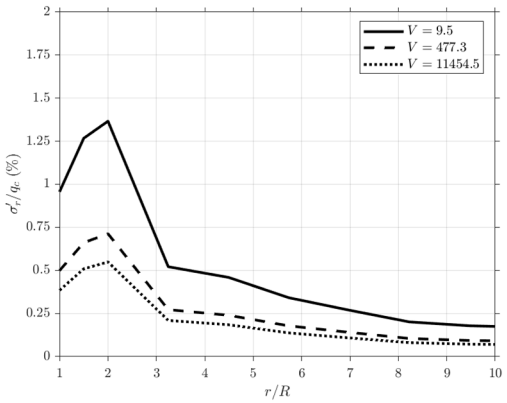

Figure 6. Post-penetration distribution of normalised radial effective stress (σ_r'/q_c) against normalised distance to cone central axis (r/R)

5 SUMMARY AND CONCLUSIONS

This study demonstrates the capability of a coupled hydro-mechanical CEL method for simulating rate-dependent cone penetration in dense fine silica sands. By incorporating a hypoplastic soil model, the approach successfully captures the evolution and distribution of excess pore pressure and radial effective stress during and post-cone penetration. The findings are essential for improving the understanding and modelling of cone and pile penetration behaviour in saturated media. The coupled CEL method provides a robust large-deformation modelling framework with potential applications in a range of offshore penetration and installation problems in challenging soils.

6 ACKNOWLEDGEMENTS

The first Author gratefully acknowledges financial support from the University of Bristol through a Global Challenges Doctoral Scholarship, as well as the kind guidance of Professor Patrick Staubach of Bauhaus-Universität Weimar on the implementation of the VUMAT subroutine.

7 REFERENCES

Augarde, C. E., Lee, S. J. & Loukidis, D. 2021. Numerical modelling of large deformation problems in geotechnical engineering: A state-of-the-art review. *Soils and Foundations* 61(6), 1718-1735.

Benson, D. J. 1992. Computational methods in Lagrangian and Eulerian hydrocodes. Computer methods in Applied mechanics and Engineering 99(2-3), 235-394.

Bienen, B., Henke, S. and Pucker, T. 2011. Numerical study of the bearing behaviour of circular footings penetrating into sand. *Proceedings 13th International Conference Int. Ass. for Computer Methods and Advances in Geomechanics (IACMAG)*, 939-944.

Chow, S. H., Diambra, A., O'Loughlin, C. D., Gaudin, C. and Randolph, M. F. 2020. Consolidation effects on monotonic and cyclic capacity of plate anchors in sand. *Géotechnique* 70(8): 720-731.

Chow, S. H., Roy, A., Herduin, M., Heins, E., King, L. Bienen, B., O'Loughlin, C. D., Gaudin, C. & Cassidy, M. J. 2019. Characterisation of UWA superfine silica sand. *Oceans graduate*

Chow, S. H., Bienen, B. and Randolph, M. F. 2018. Rapid penetration of piezocones in sand. *Cone penetration testing 2018*, 213-219.

Dassault Systèmes 2023. Abaqus User's Manual.

Hamann, T., Qiu, G. and Grabe, J. 2015. Application of a Coupled Eulerian–Lagrangian approach on pile installation problems under partially drained conditions. *Computers and Geotechnics* 63(2015), 279-290.

Jardine, R. J., Zhu, B. T., Foray, P. & Yang, Z. X. (2013). Interpretation of stress measurements made around closed-ended displacement piles in sand. *Géotechnique*, 63(8), 613-627.

Jardine, R. J. 2023. Time-dependent vertical bearing behaviour of shallow foundations and driven piles. 6th ISSMGE McClelland Lecture. Proc. 9th Int. Conf. on Offshore Site Investigations and Geotechnics, SUT, London, pp. 27–81.

Jardine, R. J., Chow, F. C., Overy, R. and Standing, J. R. 2005. ICP design methods for driven piles in sands and clays, Thomas Telford, London

Kalourazi, A. F., Liu, T., Diambra, A., Mylonakis, G. and Tian, Y. 2025. Application of coupled hydro-mechanical CEL method for variable rate cone penetration analysis. *5th Int. Symposium on Frontiers in Offshore Geotechnics*, Nantes, 795-800.

Konkol, J. 2014. Numerical solutions for large deformation problems in geotechnical engineering. *PhD Interdisciplinary Journal* 1(2014), 49-55.

Liu, T., Vinck, K., Jardine, R. J., Kontoe, S. & Bucklesy, R. M. (2025) The reliability of axial design methods for open steel piles driven in chalk. *Journal of Geotechnical and Geoenvironmental Engineering*, 151(12).

Niemunis, A. and Herle, I. 1997. Hypoplastic model for cohesionless soils with elastic strain range. *Mechanics of Cohesive-frictional Materials: An International Journal on Experiments, Modelling and Computation of Materials and Structures* 2(4), 279-299.

Noh, W. F., 1963. CEL: A time-dependent, two-space-dimensional, coupled Eulerian-Lagrange code (No. UCRL-7463). Lawrence Radiation Lab., Univ. of California, Livermore.

Qiu, G., Henke, S. and Grabe, J. 2011. Application of a Coupled Eulerian–Lagrangian approach on geomechanical problems involving large deformations. *Computers and Geotechnics* 38(1), 30-39. *school technical report*, Geo 18844. Perth, Australia: The University of Western Australia.

Stapelfeldt, M., Bienen, B. and Grabe, J. 2020. The influence of the drainage regime on the installation and the response to vertical cyclic loading of suction caissons in dense sand. *Ocean Engineering*, 215(2020), 107105.

Staubach, P., Machaček, J., Moscoso, M. C. and Wichtmann, T. 2020. Impact of the installation on the long-term cyclic behaviour of piles in sand: A numerical study. *Soil Dynamics and Earthquake Engineering* 138(2020), 106223.

Staubach, P., Machaček, J., Skowronek, J. and Wichtmann, T. 2021. Vibratory pile driving in water-saturated sand: Back-analysis of model tests using a hydro-mechanically coupled CEL method. *Soils and foundations* 61(1), 144-159.

Von Wolffersdorff, P. A. 1996. A hypoplastic relation for granular materials with a predefined limit state surface. *Mechanics of Cohesive-frictional Materials: An International Journal on Experiments, Modelling and Computation of Materials and Structures* 1(3), 251-271.

Wang, D., Bienen, B., Nazem, M., Tian, Y., Zheng, J., Pucker, T. and Randolph, M. F. 2015. Large deformation finite element analyses in geotechnical engineering. *Computers and geotechnics* 65(2015), 104-114.

Yang, Z. X., Gao, Y. Y., Jardine, R. J., Guo,W. B. and Wang, D. 2020. Large deformation finite element simulation of displacement pile installation experiments in Sand. *Journal of Geotechnical and Geoenvironmental Engineering*, 146(6): 04020044.

Ye, R. R., Huang, Z. Y., Yang, Z. X., Guo, N., Jardine, R. J. and Fu, S. 2024. Large deformation analysis of intermittent pile penetration into dense sand incorporating a state-dependent Mohr–Coulomb model. *Canadian Geotechnical Journal* 62, 1-23.

Yi, J. T., Goh, S. H., Lee, F. H. and Randolph, M. F. 2012. A numerical study of cone penetration in fine-grained soils allowing for consolidation effects. *Géotechnique* 62(8), 707-719.

Zienkiewicz, O. C. and Shiomi, T. 1984. Dynamic behaviour of saturated porous media; the generalized Biot formulation and its numerical solution. *International journal for numerical and analytical methods in geomechanics* 8(1), 71-96.